# Greenland Ice Cores Reveal a South-To-North Difference in Holocene Thermal Maximum Timings

Kaden C. Martin, Christo Buizert, Ed Brook, Olivia L. Williams, Jon S. Edwards, Ben Riddell-Young, T. J. Fudge, Farhana Mederbel, Ross Beaudette, Jeff Severinghaus, et al.

Geophysical Research Letters

RESEARCH LETTER
10.1029/2024GL111405

# Greenland Ice Cores Reveal a South-To-North Difference in Holocene Thermal Maximum Timings

**Kaden C. Martin[1,2], Christo Buizert[1], Ed Brook[1], Olivia L. Williams[1], Jon S. Edwards[1], Ben Riddell-Young[1,3], T. J. Fudge[4], Farhana Mederbel[5], Ross Beaudette[6], Jeff Severinghaus[6], Ikumi Oyabu[7], Kenji Kawamura[7], Marie Kirk[8], Iben Koldtoft[8], J. P. Steffensen[8], and Thomas Blunier[8]**

[1]College of Earth, Ocean, and Atmospheric Sciences, Oregon State University, Corvallis, OR, USA, [2]Woods Hole Oceanographic Institution, Falmouth, MA, USA, [3]Cooperative Institute for Research in Environmental Sciences, University of Colorado, Boulder, Boulder, CO, USA, [4]Department of Earth and Space Sciences, University of Washington, Seattle, WA, USA, [5]Université de Versailles Saint Quentin en Yvelines, University of Paris, Saclay, Versailles, France, [6]Scripps Institution of Oceanography, University of California, San Diego, CA, USA, [7]National Institute of Polar Research, Research Organization of Information and Systems, Tokyo, Japan, [8]University of Copenhagen, Copenhagen, Denmark

**Key Points:**

- We identify a Holocene Thermal Maximum (HTM) across three Greenland ice cores of 1.6–2.6°C above pre-industrial
- The HTM has a south-to-north difference in timing, beginning earlier at Greenland Ice Sheet Project 2 in the south (9.9 ka) and later at NEEM in the north (6.85 ka)
- Total air content suggests that deglacial elevation change contributes to this timing difference, but cannot fully explain observed trends

**Supporting Information:**

Supporting Information may be found in the online version of this article.

**Correspondence to:**

K. C. Martin,
kaden.martin@whoi.edu

**Citation:**

Martin, K. C., Buizert, C., Brook, E., Williams, O. L., Edwards, J. S., Riddell-Young, B., et al. (2024). Greenland Ice cores reveal a south-to-north difference in Holocene thermal maximum timings. *Geophysical Research Letters*, *51*, e2024GL111405. https://doi.org/10.1029/2024GL111405

Received 18 JUL 2024
Accepted 28 NOV 2024

**Abstract** Holocene temperature evolution remains poorly understood. Proxies in the early and mid-Holocene suggest a Holocene Thermal Maximum (HTM) where temperatures exceed the pre-industrial, whereas climate models generally simulate monotonic warming. This discrepancy may reflect proxy seasonality biases or errors in climate model internal feedbacks or dynamics. Using seasonally unbiased ice core reconstructions at NEEM, NGRIP, and Greenland Ice Sheet Project 2, we identify a Greenland HTM of ~2°C above pre-industrial, in agreement with other Northern Hemisphere proxy reconstructions. The firn-based reconstructions are verified through borehole thermometry, producing a multi-core, multi-proxy reconstruction of Greenland climate from the last glacial to pre-industrial. HTM timing across Greenland is heterogenous, occurring earlier at high elevations. Total air content measurements suggest a temperature contribution from elevation changes; regional oceanographic conditions, a weakened polar lapse rate, or variable near-surface inversions may also be important sensitivities. Our reconstructions support climate simulations with dynamic Holocene vegetation, highlighting the importance of vegetation feedbacks.

**Plain Language Summary** Climate change during the Holocene, the current geological time period, is important to understand. This period began ~11.7 thousand years ago and contains the transition from the last ice age to today. Simulations of this transition suggest that global climate continued to warm across this whole period. Proxy evidence, however, tends to suggest that warmer-than-modern temperatures were reached at the start of the Holocene, followed by gradual cooling. Resolving this dispute in our recent climatological past is important to verify climate model behavior, and understand nuances in proxy records. Using ice core reconstructions of Greenland climate, which broadly follows northern high-latitude climate, we lend further support to a warm period in the early Holocene. These new records are spread across Greenland, allowing for the spatial fingerprint of this warm period to be identified.

## 1. Introduction

The Holocene (11.7 ka to present) is a critical period to characterize, as it provides a historic context for contemporary anthropogenic climate change (Fischer et al., 2018; Lüning & Vahrenholt, 2017). Across this period, climate models tend to simulate a monotonic warming trend in global mean surface temperature (GMST) initiating at Holocene onset and continuing until pre-industrial conditions (Liu et al., 2014). Proxy compilations of GMST, however, suggest that peak temperatures exceeding the pre-industrial were reached in the early- to mid-Holocene (the Holocene Thermal Maximum, or HTM), followed by a cooling trend through the late Holocene (Marcott et al., 2013). This model-data discrepancy, dubbed the "Holocene Temperature Conundrum" (Liu et al., 2014), is the possible result of seasonally biased (Bova et al., 2021) or poorly distributed proxy networks, incorrect model sensitivities, or inaccurate representation of key climate feedbacks in models (Kaufman & Broadman, 2023). Recent model studies have simulated a HTM, driven primarily through the albedo effect of expanding Saharan, mid-latitude, and Arctic vegetation (Thompson et al., 2022). Reduced atmospheric dust loading, a consequence of Holocene vegetation change, further allow models to better simulate a HTM (Liu et al., 2018).

While expressed globally, the HTM is most pronounced in the northern high latitudes (Cartapanis et al., 2022). Evidence of warmer than pre-industrial temperatures is widespread across the Arctic, appearing in records of glacier and ice-cap extent, ice core records, pollen, among other marine and terrestrial proxies. While nearly all records indicate a cooling trend during the late Holocene, they suggest different regional timings for the onset of HTM conditions across the Arctic (Axford et al., 2021; Briner et al., 2016). Greenland and eastern Canadian records indicate that regions north of ∼66°N express warmer than pre-industrial temperatures during the early-Holocene, whereas southward this occurs during the mid-Holocene. Peak summer temperatures are typically reached earlier in western and central Canada and Alaska than for Greenland (Gajewski, 2015; Kaufman et al., 2004). Regional variability is superimposed on this wider pattern. For instance, both Baffin Bay and the Labrador Sea exhibit a delayed HTM onset during the mid Holocene (Briner et al., 2016; Hansen et al., 2020). Ice-caps and glacier systems are particularly sensitive to HTM conditions, showing rapid retreat during the early Holocene (Larocca & Axford, 2022) despite nearby marine environments suggesting colder conditions. This pattern of regionally variable HTM onset highlights the unique interactions of deglacial climate forcings across the northern high-latitudes, with meltwater, ocean circulation and sea ice variability, intense increases in summer insolation, and ice sheet variations playing key roles. As model simulations struggle to resolve these observed patterns across the northern high-latitudes (Zhang et al., 2017), this highlights the importance of correctly resolving transient deglacial climate forcings (Zhang et al., 2018).

Within the central Greenland ice core record, reconstructions using water isotopes ($\delta^{18}O$), a widely used but relatively qualitative proxy for site temperature, do not identify a strong HTM. Instead, central Greenland $\delta^{18}O$ suggests elevated, but stable, temperatures from the early Holocene through the pre-industrial. Borehole thermometry reconstructions from central and southern Greenland (GRIP and Dye 3, respectively) have identified a strong HTM with subsequent cooling. These reconstructions indicate the timing of the HTM differs between sites in central Greenland and those near the boundaries of the ice sheet (Dahl-Jensen et al., 1998). Central Greenland likely reflects a similar temperature history to other Arctic sites at similar latitudes (Briner et al., 2016), while temperature records sourced near the ice sheet margins are susceptible to overprinting by elevation-driven temperature variability (Lecavalier et al., 2017; Vinther et al., 2009). Northwest Greenland is particularly sensitive to this effect, as it likely underwent a larger elevation change via the loss of buttressing support following the collapse of the ice saddle to the Innuitian Ice sheet (Lecavalier et al., 2017).

Interpreting the differing regional patterns of Holocene temperature across Greenland and the Canadian Arctic would be aided by alternative, mean-annual temperature ice core reconstructions from central Greenland. Here, we develop a seasonally unbiased temperature and accumulation reconstruction through an inverse firn-modeling method to investigate Greenland climate evolution at three sites from the Last Glacial Maximum (LGM) through the Holocene.

## 2. Methods

### 2.1. Records Produced

We present new measurements of atmospheric $CH_4$ mixing ratios and the isotopic $^{15}N/^{14}N$ ratio in $N_2$ ($\delta^{15}N$) in the GISP2, North Greenland Ice Core Project (NGRIP), and North Greenland Eemian Ice Drilling (NEEM) ice cores (Figure 1). $CH_4$ measurements were conducted on 129, 51, and 34 sampling depths for NEEM, NGRIP, and GISP2 respectively at Oregon State University via wet-extraction (Lee et al., 2020; Mitchell et al., 2013). For $\delta^{15}N$, 48, 28, and 5 sampling depths in NEEM, NGRIP, and GISP2 respectively were measured at the Ice Core Noble Gas Laboratory of the Scripps Institution of Oceanography using established wet-extraction techniques (Buizert et al., 2014; Kobashi et al., 2008). An additional 207 NEEM sample depths were measured at the National Institute of Polar Research, similarly utilizing a wet-extraction technique (Oyabu et al., 2020). The total records used here are a combination of previously published data and new measurements (Figures S1–S3 in Supporting Information S1).

### 2.2. Bipolar $CH_4$ Synchronization and Firn Model Reconstructions

Centennial and millennial-scale $CH_4$ variability can be used to synchronize the gas-age scales of different ice cores (Blunier & Brook, 2001; Blunier et al., 1998). We target such periods to synchronize NGRIP and NEEM

10.1029/2024GL111405

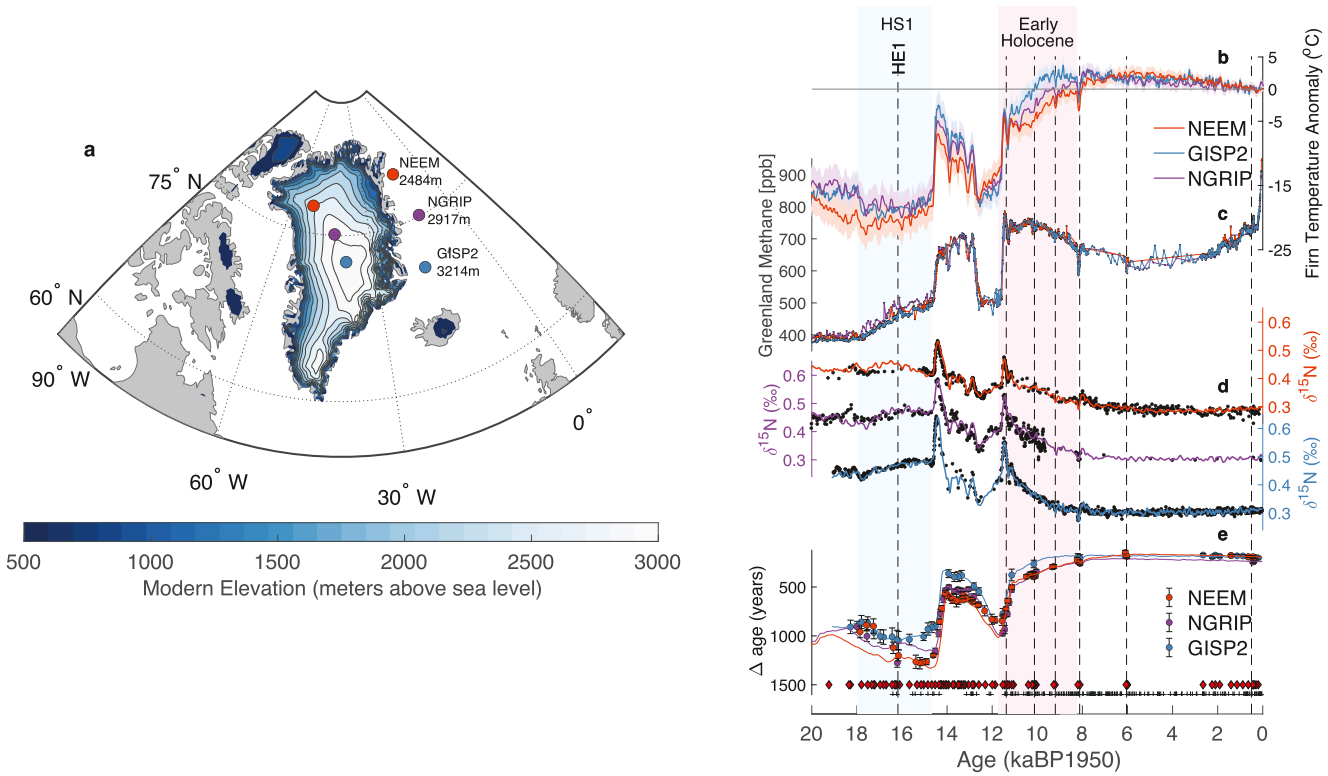


**Figure 1.** Greenland climate records produced in this study. (a) Modern ice sheet elevation across Greenland (Box et al., 2009). (b) Modeled temperature anomaly for NEEM (orange), NGRIP (purple), and Greenland Ice Sheet Project 2 (GISP2) (blue), referenced to the 500-year average between 200 and 700 yrBP. Shaded regions are Δage-based uncertainty following the method of (Buizert, 2021). (c) NEEM $CH_4$ (orange, this study and Dahl-Jensen et al., 2013; Rhodes et al., 2013; Rosen et al., 2014), NGRIP $CH_4$ (purple, this study and Baumgartner et al., 2014; Beck et al., 2018), and GISP2 $CH_4$ (blue, this study and Martin et al., 2023; Mitchell et al., 2013; Seierstad et al., 2014). (d) NEEM $\delta^{15}N$ (this study and Guillevic, 2013; Oyabu et al., 2020; Rosen et al., 2014), NGRIP $\delta^{15}N$ (this study and Kindler et al., 2014), and GISP2 $\delta^{15}N$ (this study and Martin et al., 2023; Seierstad et al., 2014). For $\delta^{15}N$, model reconstructions are in respective colors and data in black. (e) Δage at NEEM (orange, this study), NGRIP (purple, this study), and GISP2 (blue, this study and Martin et al., 2023). For Δage, empirical constraints are in circles, and model reconstruction are in lines; note reversed scale. Red diamonds indicate gas-phase matches via $CH_4$, plus signs (+) indicate bipolar ice-phase matches via volcanic synchronization. Vertical dashed lines indicate key periods of shared $CH_4$ variability used to constrain Δage.

with GISP2 and the West Antarctic Ice sheet Divide (WD) ice core (Figure 1). We identify 33 gas-phase tie points during the Holocene, and 43 from HS1 onset to the Younger Dryas termination—though not all ties are present in all cores. The ice-age scales are synchronized to WD through 187 bipolar volcanic matches during the glacial (Svensson et al., 2020) and Holocene (Sigl et al., 2022; Veres et al., 2013). There are 839 GISP2-NGRIP and 737 NEEM-NGRIP ice-phase ties used to transfer bipolar matches across Greenland (Rasmussen et al., 2013; Seierstad et al., 2014). With both gas- and ice-phase chronologies well constrained, the Δage (the gas-age–ice-age difference) can be empirically estimated.

To reconstruct Greenland temperature and accumulation, we utilize an inverse dynamical firn densification strategy. A detailed description of the firn model is provided in (Buizert et al., 2014; Martin et al., 2023). Briefly, a coupled firn densification and heat diffusion model using a dynamic description of the Herron-Langway model simulates the response of the firn layer to climate at the site (Herron & Langway, 1980). The forward model scenario utilizes site surface temperature ($T_{site}$) and accumulation rate (Acc) to generate an output of $\delta^{15}N$ and Δage. We employ the inverse mode, running the forward model repeatedly to find $T_{site}$ and Acc histories that optimize the fit of simulated $\delta^{15}N$ and Δage histories with data. The initial guess for $T_{site}$ and Acc is based on a "climate template" at each site, composed of each record's average $\delta^{18}O$ and $Ca^{2+}$. The $Ca^{2+}$ values are scaled to an equivalent change in $\delta^{18}O$, improving the signal-to-noise-ratio. The climate template is the composite of $\delta^{18}O$ and $Ca^{2+}$ during the last glacial (11.7 ka and older). For the Holocene (11.7 ka and younger) only $\delta^{18}O$ is used. Temperature and accumulation values are scaled from the template via the reconstructions of (Buizert et al., 2014).

## 3. Results

### 3.1. Firn Model Temperature Reconstructions

Reconstructed site temperature histories characterize a unique Greenland climate evolution (Figure 1a), with a south-to-north difference in the magnitude and pacing of temperature change. We define that a record reaches the HTM when 500-year averaged temperature exceeds half of the peak-Holocene−pre-industrial difference (the HTM threshold). Anomalies are relative to the average of 0.2–0.7 kaBP, allowing for a 500-year reference period.

The south-to-north HTM difference is characterized by rapid warming at GISP2 and more gradual warming at NEEM (Table S1 in Supporting Information S1). All three sites reach peak temperatures between 1.5 and 2.5°C above pre-industrial, but differ in structure. The onset of the HTM at GISP2 is at 9.88 ka, exceeding the HTM threshold of 1.24°C. NEEM is the latest, exceeding the HTM threshold of 0.8°C by 6.85 ka. NGRIP has an intermediate structure, with a HTM threshold of 1.3°C by 8.0 ka. Elevated temperatures are sustained through the mid-Holocene for all three sites, with cooler than pre-industrial values only reached during the period of 1 and 0 ka.

Our reconstructions extend from the late LGM through Heinrich Stadial 1 (HS1). We observe rapid depletions in NEEM and NGRIP $\delta^{15}N$ at HS1 onset which suggests cooling. The $\Delta$age likewise increases, suggesting cold, arid conditions at the sites (Figure 1e). Model reconstructions, however, only capture broad features across HS1. Comparatively sparse data coverage during the LGM-HS1 transition likely causes this, as the climate template has a stronger influence on the reconstruction. As such, we refrain from assigning a precise magnitude to the HS1 onset. The magnitude of the well-constrained GISP2 cooling of 3°C likely represents the upper limit of HS1 onset cooling at NEEM and NGRIP (Martin et al., 2023).

### 3.2. Verification Through Borehole Thermometry

We utilize borehole thermometry to verify our reconstructed temperature and accumulation histories. We are not performing an inversion to reconstruct the temperature history (e.g., Cuffey et al., 1995; Dahl-Jensen et al., 1998); instead, we test whether the firn model reconstructions are consistent with borehole temperatures. We force a one-dimensional heat transport-ice flow model with the firn temperature and accumulation histories (Buizert et al., 2021). The surface temperature, shape of the vertical velocity profile, and either the geothermal flux or basal melt rate can adjust as free parameters (Table S2 in Supporting Information S1). The misfit between the firn-derived ice-flow reconstructions and the measured borehole temperatures (Løkkegaard et al., 2023) then informs the accuracy of the firn-model histories.

For NEEM, NGRIP, and GISP2, the ice-flow model accurately fits the borehole temperature with realistic glaciological parameters (Figure S4 in Supporting Information S1). GISP2 exhibits the best fit, with an average misfit of ±0.029°C between borehole measurements and reconstructions. NGRIP and NEEM are more challenging, as variable depositional environments and deeper folding are indicative of complex flow regimes. For NGRIP, we reconstruct observed borehole values within ±0.042°C. NEEM is complicated by possible convection of deeper borehole fluid (Figure S4 in Supporting Information S1). Here, we reconstruct observed borehole values within ±0.087°C; excluding the deep disturbance, the fit is within ±0.037°C. These results support our reconstructions as consistent with the borehole measurements, however they are limited by complexity in the deep borehole.

### 3.3. Comparisons With Proxies and Models

Assessing terrestrial (Marsicek et al., 2018; Zhang et al., 2022) and marine (Bova et al., 2021; Marcott et al., 2013) reconstructions provides insight into potential modulating components of early Holocene climate at our sites (Figure 2). Marine reconstructions share a similar timing with GISP2, as both exceed modern temperatures within 200 years of each other and reach HTM values before 8 ka. The (Marcott et al., 2013) reconstruction exceeds modern temperatures at a similar timing to the northern high-latitude Temp12k reconstruction (Kaufman et al., 2020), and likewise stabilizes between 9.8 ka and 9.6 ka. Terrestrial pollen reconstructions (Marsicek et al., 2018; Zhang et al., 2022) exhibit later timings, with the fastest exceeding modern values by 8.4 ka and reaching peak values by 7 ka. Temperature evolution at NEEM is more similar to the terrestrial reconstructions, as HTM values are reached during the mid-Holocene. NGRIP is of an intermediate structure; its HTM onset precedes the terrestrial reconstructions but lags the marine. For all three sites, the magnitude of peak warming is

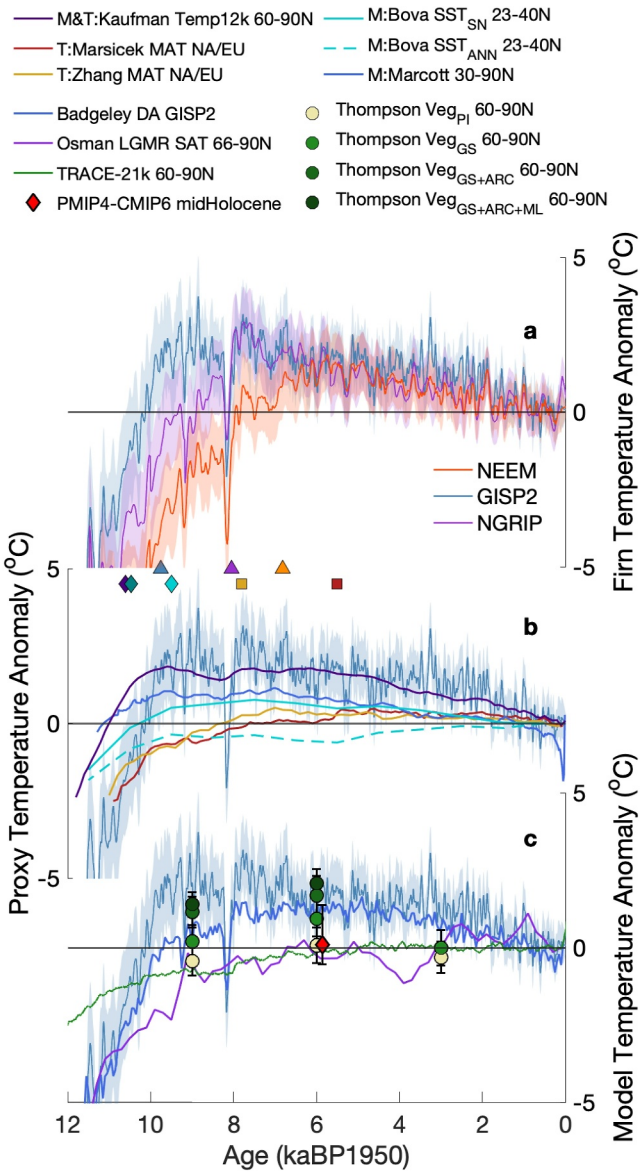


**Figure 2.** Comparison between Greenland temperature and other reconstructions over the Holocene. (a) Site temperature anomaly for NEEM (orange), NGRIP (purple), and Greenland Ice Sheet Project 2 (GISP2) (blue). (b) Proxy reconstructions of northern high-latitude temperature variability: GISP2 firn reconstruction for reference (shading denotes Δage-based uncertainty; blue), Temp12k (purple, Kaufman et al., 2020), terrestrial mean annual temperatures (red, Marsicek et al., 2018; gold, Zhang et al., 2022), and marine reconstructions (teal, Bova et al., 2021; blue, Marcott et al., 2013). Markers in panel b indicate when marine and Temp12k (diamond), terrestrial (square), and ice core (triangle) reconstruction exceed the Holocene Thermal Maximum threshold defined in Section 3.1. (c) Transient and equilibrium model experiments of northern high-latitude variability: GISP2 firn reconstruction (blue), data assimilation reconstructions (dark blue, Badgeley et al., 2020; purple, Osman et al., 2021), transient deglacial simulations (green, Liu et al., 2014) PMIP4-CMIP6 equilibrium scenarios (red diamond, Brierley et al., 2020), and varied vegetation equilibrium scenarios (beige and green circles, Thompson et al., 2022).

similar to the Temp12k reconstruction. However, the rate of warming during the early Holocene in Temp12k is only comparable at GISP2. The broad agreement across different archives supports that our observed Greennland temperature variability aligns with both the range of onset timings and magnitude of the HTM across the northern high latitudes (Cartapanis et al., 2022; Kaufman et al., 2020).

While within the range of zonal Arctic trends, comparisons with other records across Greenland and the eastern Canada reveal regional nuances. There is a reversal between GISP2 and NEEM's latitude within the observed trends (Briner et al., 2016), where warmer than pre-industrial temperatures are reached later farther north. However, this trend is established by only a few sites which include ice core records. Records of glacier and ice-cap variability in northwest Greenland indicate significantly reduced extent in the early-Holocene, suggesting strong early warming (Larocca & Axford, 2022). In contrast, marine records from northeast Baffin Bay suggest colder conditions with more extensive sea ice cover through the early- Holocene, reaching warmer conditions during the mid-Holocene (Briner et al., 2016; Hansen et al., 2020). Pollen records from northeastern Canada and northwest Greenland similarly suggest that warmer conditions were reached only in the mid-Holocene (Gajewski, 2015). Our mean-annual reconstruction from NEEM aligns with records from north Greenland which indicate peak warming during the mid-Holocene, rather than the early-Holocene. Terrestrial pollen and glaciological records at similar latitudes to GISP2 and NGRIP are consistent with the observed timings of peak warmth during the early- to mid-Holocene (Axford et al., 2021; Gajewski, 2015; Larocca & Axford, 2022). However, these terrestrial timings contradict marine records from the Greenland and Labrador Sea which suggest delayed warming during the mid-Holocene.

Transient climate simulations and the midHolocene PMIP4-CMIP6 benchmark experiments (Brierley et al., 2020) do not reproduce the trends observed in the ice core reconstructions (Figure 2c). Studies utilizing DA have sought to resolve the Holocene Temperature Conundrum through model-data synthesis (Erb et al., 2022; Osman et al., 2021). The global DA reconstructions support the model perspective of monotonic Holocene warming, failing to capture the HTM identified in our ice core reconstructions. The Greenland-specific DA reconstruction of (Badgeley et al., 2020) does reproduce a HTM in the mid-Holocene. The DA reconstruction of (Osman et al., 2021) suggests agreement only within the uppermost bound (97.5%) of the posterior and the lowest bound (2.5%) of the proxy records. The DA reconstruction of (Erb et al., 2022) similarly shows that assimilated temperatures are at the upper limit of model prior variability. Both results suggest that the distribution width of the model priors is insufficient to capture the HTM evident in proxies.

Equilibrium model experiments implementing more expansive Northern Hemisphere vegetation scenarios (Thompson et al., 2022) produces a mid-Holocene HTM in agreement with proxy reconstructions. However, these simulations overestimate the early-Holocene Greenland temperature response (Figure S5 in Supporting Information S1) and don't express wider Arctic trends. Despite this, the reproduced mid-Holocene HTM suggests that terrestrial vegetation feedbacks may play an important role in amplifying insolation driven climate changes during early interglacial periods alongside glacial inceptions (Willeit et al., 2024). Orbitally-driven vegetation change

may therefore be an important driver of Earth's glacial cycles, in parallel to the more widely recognized ice volume response.

## 4. Possible Drivers of the Greenland HTM Temperature Difference

### 4.1. Elevation Variability

Greenland ice core temperature reconstructions contain an imprint of elevation change via the temperature lapse rate, which has not yet been sufficiently constrained. One method to constrain this assumes that Holocene climate variability across Greenland is homogenous, and that the residual between an ice core record and a reference core with stable elevation history reflects the former's elevation history (Vinther et al., 2009). Another uses ice flow models. These include complex ice sheet and glacial isostatic adjustment models that are forced by ice core records and Arctic relative sea level constraints, such as the Huy3 model (Lecavalier et al., 2014), and simple one-dimensional ice-flow models that are predominately sensitive to the extent of margin retreat during the deglaciation (Cuffey & Clow, 1997).

Assuming that temperature differences between cores can be fully explained via elevation changes, the temperature anomaly between NEEM and GISP2 can be converted to a putative elevation anomaly via the 7.1°C/km temperature lapse rate (Steffen & Box, 2001). Between 10.4 and 9.8 ka the maximum NEEM-GISP2 temperature difference would imply that NEEM-GISP2 elevation difference was 690 ± 70 m smaller relative to today, nearly eliminating their modern 730 m elevation difference. This would imply a near-absent surface slope across central to northwest Greenland, with ∼40 m of elevation change across the 640 km horizontal distance between the sites. In contrast, ice sheet models suggests that NEEM was only ∼60 m higher in elevation during the early Holocene relative to today (Lecavalier et al., 2014).

We can assess these contrasting results via measurements of the total air content (TAC; Figure 3; Supplement). The TAC in ice core samples was originally explored as a paleo-elevation proxy, reflecting changes in atmospheric pressure (Martinerie et al., 1992). However, it is a complex proxy influenced by several competing effects including integrated summer insolation (ISI; Eicher et al., 2016; Raynaud et al., 2007), abrupt temperature changes, accumulation variability, firn conditions and possibly summer temperature (Eicher et al., 2016; Epifanio et al., 2023; Raynaud et al., 2023).

Independently, TAC is unlikely to predict elevation due to the competing factors. However, TAC differences between sites provides insight into relative elevation changes, as the confounding influences are expected to be comparable at these sites (Buizert et al., 2021). To investigate the relative elevation changes between NEEM and GISP2, we examine the difference in the 500-year binned average of TAC (ΔTAC). A 500-year binning is utilized to limit the impact of short-lived climate variations while still resolving millennial-scale trends. We note a period of reduced ΔTAC between 9 and 8 ka, which is likely the result of abrupt cooling associated with the 9.2 ka (Fleitmann et al., 2008) and 8.2 ka events. The sensitivity of TAC to ISI has been quantified at a value between −5.7 and −6.6 mL $kg^{-1}$ $GJ^{-1}$ (Eicher et al., 2016; Raynaud et al., 2007). This sensitivity can explain most of the long-term TAC trend at these sites, yet not the differences between the sites.

We consider two possible endmember scenarios: (a) If NEEM was similar in elevation to GISP2 during the LGM and early Holocene and transitioned to the modern elevation difference by the mid Holocene, LGM ΔTAC would be zero and then gradually increase to the modern value during the mid Holocene. (b) If the elevation difference between the sites was stable, ΔTAC would also remain stable at the modern value.

The ΔTAC lies inbetween the two endmembers, suggesting a reduced, but stable, elevation difference (Figure 3d). Early to mid-Holocene ΔTAC is 28.5% smaller than the modern difference (4.63 and 6.48 mL $kg^{-1}$ respectively), suggesting a reduced NEEM-GISP2 elevation difference through the early Holocene. Applying a linear scaling of modern ΔTAC and elevation difference, the early Holocene ΔTAC suggests a stable 521 ± 120 m elevation difference between NEEM and GISP2. This suggests that large changes in elevation are not the dominant driver of the HTM temperature difference between our sites, as there is no transient lowering of NEEM elevation which could drive gradual warming. Increased elevation does play a role in suppressing early Holocene warmth at NEEM, but this effect is stable through the early Holocene. In our estimate, this explains −1.48°C of the total −4.9°C temperature difference at a 7.1°C/km lapse rate.

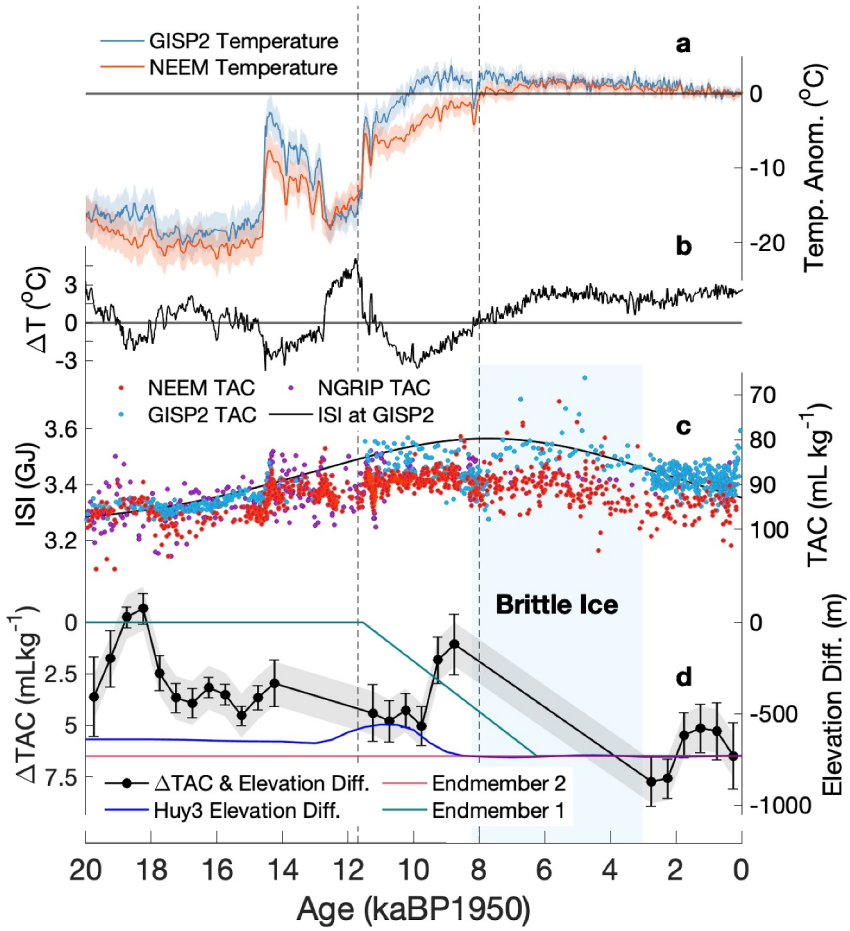


**Figure 3.** Greenland site temperature and total air content. (a) NEEM and Greenland Ice Sheet Project 2 (GISP2) temperature anomaly (orange, blue). (b) Temperature difference between NEEM and GISP2 (black). (c) Right: Total air content (TAC; units of mL kg$^{-1}$) for NEEM (orange, this study and Rhodes et al., 2013; Rosen et al., 2014), NGRIP (purple, this study and Eicher et al., 2016), and GISP2 (blue, this study and Martin et al., 2023; Mitchell et al., 2013). Left: Integrated summer insolation (ISI) at GISP2 (Berger & Loutre, 1991). (d) Left: Difference in 500-year binned TAC between NEEM and GISP2. Right: transient NEEM-GISP2 elevation difference scaled from modern the TAC/Elevation relationship. NEEM-GISP2 elevation difference from the Huy3 model (blue; Lecavalier et al., 2014). Endmembers associated with different elevation histories (teal, orange). Error bars are the average standard deviation of TAC within the GISP2 and NEEM 500-year bin. Shaded area is the error estimate for elevation, based on the variability of the modern relationship. Vertical dashed lines indicate the early Holocene.

This result contradicts studies utilizing TAC as a proxy for large elevation changes (Vinther et al., 2009) and the ice sheet modeling studies which suggest a more limited elevation variability within the Greenland interior (Lecavalier et al., 2014). Our results suggest an intermediate scenario, with a transition from a reduced LGM elevation difference to an elevation difference similar to (Lecavalier et al., 2014) during the early Holocene. The modern elevation difference is then established during the mid to late Holocene, likely not before 8 kaBP. Unfortunately, systematic gas loss through the brittle ice zone (Figure 3) precludes a precise timing of when the modern elevation difference is established via the TAC method.

### 4.2. Other Drivers of the Greenland HTM Temperature Difference

As elevation cannot fully explain the differences across our Greenland reconstructions, other mechanisms must contribute. One possibility is a changing lapse rate. Our reconstructions are consistent with an elevation-dependent temperature sensitivity (Pepin et al., 2015), where LGM cooling is weakest and HTM warming is greatest at high elevation (Figure S6 in Supporting Information S1). Recent Antarctic LGM cooling reconstructions (Buizert et al., 2021) also scale strongly with site elevation (Figure S4 in Supporting

Information S1). This suggests the possibility of a weak polar lapse rate through the LGM and early Holocene, in alignment with proxy and modeled lapse rate reconstructions (Legrain et al., 2023). This shallow lapse rate can be produced by enhanced moisture content during Holocene warming (Legrain et al., 2023; Rangwala & Miller, 2012). During the LGM, it could be driven by increased high-altitude meridional heat transport (Hwang & Frierson, 2010; Yang et al., 2010) or by reduced cloudiness (Cronin & Jansen, 2016). This supports heterogeneity in global LGM lapse rates (Legrain et al., 2023), and provides spatial contrast to tropical reconstructions (Loomis et al., 2017) of strong LGM lapse rates. Low elevation Dye3 and Camp Century also have a late HTM, but Renland does not (Vinther et al., 2008, 2009); this could be the result of differing controls on $\delta^{18}O_{ice}$ variability.

Regional oceanographic conditions have been shown to amplify simulated mid-Holocene temperatures (Masson-Delmotte et al., 2006). The delayed HTM timing at NEEM could reflect its sensitivity to Baffin Bay (Masson-Delmotte et al., 2015; Zheng et al., 2018), which exhibits a similar delayed timing of Holocene warming and cooling (Hansen et al., 2020). NEEM could similarly reflect regional variability paced by the final deglaciation of the Laurentide at 6 ka (Ullman et al., 2016). In contrast, GISP2 is potentially more sensitive to conditions in the North Atlantic, which exhibits an early HTM (Cartapanis et al., 2022; Kaufman et al., 2004). However, this is complicated by delayed HTM conditions in the Labrador and Greenland Seas (Briner et al., 2016).

Lastly, variations in inversions strength over Greenland could drive regional differences. Strong, stable surface-based temperature inversions enhance stratification and inhibit warming (Zhang et al., 2011). They are correlated with local moisture conditions, where dry conditions enhance inversion frequency and intensity (Miller et al., 2013). Lower accumulation at NEEM during the early Holocene could promote more frequent inversions, inhibiting early warming. The inversion mechanism could also reflect an increased presence of synoptic-scale cyclones at GISP2, contributing greater moisture and disrupting local inversions. This increase in synoptic-scale cyclones could be the result of Laurentide remnants directing storm systems, or increased cyclogenesis from warm early Holocene Atlantic waters (Jaiser et al., 2012; Vihma, 2014).

## 5. Conclusion

The HTM is a key climatic period to assess the sensitivity of both regional Greenland climate and the Greenland Ice sheet to climate forcings such as rising sea level and increasing GMST. We identify a clear HTM at GISP2, NGRIP, and NEEM, with heterogenous onset timings across the early Holocene. Evidence of delayed warming at NEEM contrasts nearby records which suggest peak early-Holocene warming (Axford et al., 2021; Larocca & Axford, 2022; Vinther et al., 2009), highlighting differing sensitivities to deglacial and seasonal climate forcings in the region. Our reconstructions further support the near-uniform HTM onset by the mid-Holocene identified across Arctic and Northern Hemisphere reconstructions. While the differences in our reconstructions have a component of deglacial elevation variability, they further highlight the impact of transient changes in local, regional, and synoptic-scale climate processes during this period of widespread warming.

## Conflict of Interest

The authors declare no conflicts of interest relevant to this study.

## Data Availability Statement

Data generated in this study including the NEEM, NGRIP, and GISP2 methane, $\delta^{15}N\text{-}N_2$, $\Delta$age, firn model reconstructions, and total air content are available at the National Science Foundation Arctic Data Center (Martin et al. (2024); https://doi.org/10.18739/A2KP7TT2N) and provided in the Supplemental Data of this paper. The firn densification model is archived at https://github.com/ChristoBuizert/DynaDens.

**Acknowledgments**

The author acknowledges financial support from the US National Science Foundation (US-NSF) through Grants 2102944 (C.B. and T.J.F.), 1702920 (C.B. and E.J.B), funding through the Global Climate Change Foundation Grant GCCF24 (C.B.), the MEXT KAKENHI (JP24H02345) (K. K. and I.O.) and the Arctic Challenge for Sustainability II (ArCS II) (JPMXD1420318865) (K.K. and I.O.). This work is a contribution to the NGRIP ice core project, which is directed and organized by the Ice and Climate Research Group at the Niels Bohr Institute, University of Copenhagen. The NGRIP ice core project is being supported by funding agencies in Denmark (SNF), Belgium (FNRS-CFB), France (IPEV, INSU/CNRS and ANR NEEM), Germany (AWI), Iceland (RannIs), Japan (MEXT), Sweden (SPRS), Switzerland (SNF) and the USA (NSF). NEEM is directed and organized by the Center of Ice and Climate at the Niels Bohr Institute and U.S. NSF, Office of Polar Programs. NEEM is supported by funding agencies and institutions in Belgium (FNRS-CFB and FWO), Canada (NRCan/GSC), China (CAS), Denmark (FIST), France (IPEV, CNRS/INSU, CEA, and ANR), Germany (AWI), Iceland (RannIs), Japan (NIPR), Korea (KOPRI), The Netherlands (NWO/ALW), Sweden (VR), Switzerland (SNF), United Kingdom (NERC) and the USA (U.S. NSF, Office of Polar Programs). Thank you to the US-NSF Ice Core Facility for the curation and preparation of GISP2 samples.

## References

Axford, Y., De Vernal, A., & Osterberg, E. C. (2021). Past warmth and its impacts during the Holocene thermal maximum in Greenland. *Annual Review of Earth and Planetary Sciences*, *49*(1), 279–307. https://doi.org/10.1146/annurev-earth-081420-063858

Badgeley, J. A., Steig, E. J., Hakim, G. J., & Fudge, T. J. (2020). Greenland temperature and precipitation over the last 20,000 years using data assimilation. *Climate of the Past*, *16*(4), 1325–1346. https://doi.org/10.5194/cp-16-1325-2020

Baumgartner, M., Kindler, P., Eicher, O., Floch, G., Schilt, A., Schwander, J., et al. (2014). NGRIP CH4 concentration from 120 to 10 kyr before present and its relation to a δ15N temperature reconstruction from the same ice core. *Climate of the Past*, *10*(2), 903–920. https://doi.org/10.5194/cp-10-903-2014

Beck, J., Bock, M., Schmitt, J., Seth, B., Blunier, T., & Fischer, H. (2018). Bipolar carbon and hydrogen isotope constraints on the Holocene methane budget. *Biogeosciences*, *15*(23), 7155–7175. https://doi.org/10.5194/bg-15-7155-2018

Berger, A., & Loutre, M. F. (1991). Insolation values for the climate of the last 10 million years. *Quaternary Science Reviews*, *10*(4), 297–317. https://doi.org/10.1016/0277-3791(91)90033-Q

Blunier, T., & Brook, E. J. (2001). Timing of millennial-scale climate change in Antarctica and Greenland during the last glacial period. *Science*, *291*(5501), 109–112. https://doi.org/10.1126/science.291.5501.109

Blunier, T., Chappellaz, J., Schwander, J., Dällenbach, A., Stauffer, B., Stocker, T. F., et al. (1998). Asynchrony of Antarctic and Greenland climate change during the last glacial period. *Nature*, *394*(6695), 739–743. https://doi.org/10.1038/29447

Bova, S., Rosenthal, Y., Liu, Z., Godad, S. P., & Yan, M. (2021). Seasonal origin of the thermal maxima at the Holocene and the last interglacial. *Nature*, *589*(7843), 548–553. https://doi.org/10.1038/s41586-020-03155-x

Box, J. E., Yang, L., Bromwich, D. H., & Bai, L. S. (2009). Greenland ice sheet surface air temperature variability: 1840-2007. *Journal of Climate*, *22*(14), 4029–4049. https://doi.org/10.1175/2009JCLI2816.1

Brierley, C. M., Zhao, A., Harrison, S. P., Braconnot, P., Williams, C. J. R., Thornalley, D. J. R., et al. (2020). Large-scale features and evaluation of the PMIP4-CMIP6 midHolocene simulations. *Climate of the Past*, *16*(5), 1847–1872. https://doi.org/10.5194/cp-16-1847-2020

Briner, J. P., McKay, N. P., Axford, Y., Bennike, O., Bradley, R. S., de Vernal, A., et al. (2016). Holocene climate change in Arctic Canada and Greenland. *Quaternary Science Reviews*, *147*, 340–364. https://doi.org/10.1016/j.quascirev.2016.02.010

Buizert, C. (2021). The ice core gas age-ice age difference as a proxy for surface temperature. *Geophysical Research Letters*, *48*(20), 1–12. https://doi.org/10.1029/2021GL094241

Buizert, C., Fudge, T. J., Roberts, W. H. G., Steig, E. J., Sherriff-Tadano, S., Ritz, C., et al. (2021). Antarctic surface temperature and elevation during the last glacial maximum. *Science*, *372*(6546), 1097–1101. https://doi.org/10.1126/science.abd2897

Buizert, C., Gkinis, V., Severinghaus, J. P., He, F., Lecavalier, B. S., Kindler, P., et al. (2014). Greenland temperature response to climate forcing during the last deglaciation. *Science*, *345*(6201), 1177–1180. https://doi.org/10.1126/science.1254961

Cartapanis, O., Jonkers, L., Moffa-Sanchez, P., Jaccard, S. L., & de Vernal, A. (2022). Complex spatio-temporal structure of the holocene thermal maximum. *Nature Communications*, *13*(1), 5662. https://doi.org/10.1038/s41467-022-33362-1

Cronin, T. W., & Jansen, M. F. (2016). Analytic radiative-advective equilibrium as a model for high-latitude climate. *Geophysical Research Letters*, *43*(1), 449–457. https://doi.org/10.1002/2015GL067172

Cuffey, K. M., & Clow, G. D. (1997). Temperature, accumulation, and ice sheet elevation in central Greenland through the last deglacial transition. *Journal of Geophysical Research*, *102*(C12), 26383–26396. https://doi.org/10.1029/96JC03981

Cuffey, K. M., Clow, G. D., Alley, R. B., Stuiver, M., Edwin, D., Cuffey, K. M., et al. (1995). Large Arctic temperature change at the Wisconsin-Holocene glacial transition. *Science*, *270*(5235), 455–458. https://doi.org/10.1126/science.270.5235.455

Dahl-Jensen, D., Albert, M. R., Aldahan, A., Azuma, N., Balslev-Clausen, D., Baumgartner, M., et al. (2013). Eemian interglacial reconstructed from a Greenland folded ice core. *Nature*, *493*(7433), 489–494. https://doi.org/10.1038/nature11789

Dahl-Jensen, D., Gundestrup, N., Gogineni, S. P., & Miller, H. (2003). Basal melt at NorthGRIP modeled from borehole, ice-core and radio-echo sounder observations. *Annals of Glaciology*, *37*, 207–212. https://doi.org/10.3189/172756403781815492

Dahl-Jensen, D., Mosegaard, K., Gundestrup, N., Clow, G. D., Johnsen, S., Hansen, A. W., & Balling, N. (1998). Past temperatures directly from the Greenland ice sheet. *Science*, *282*(October), 268–271. https://doi.org/10.1126/science.282.5387.268

Eicher, O., Baumgartner, M., Schilt, A., Schmitt, J., Schwander, J., Stocker, T. F., & Fischer, H. (2016). Climatic and insolation control on the high-resolution total air content in the NGRIP ice core. *Climate of the Past*, *12*(10), 1979–1993. https://doi.org/10.5194/cp-12-1979-2016

Epifanio, J. A., Brook, E. J., Buizert, C., Pettit, E. C., Edwards, J. S., Fegyveresi, J. M., et al. (2023). Millennial and orbital-scale variability in a 54-000-year record of total air content from the South Pole ice core. *The Cryosphere*, *17*(11), 4837–4851. https://doi.org/10.5194/tc-17-4837-2023

Erb, M. P., Mckay, N. P., Steiger, N., Dee, S., Hancock, C., Ivanovic, R. F., et al. (2022). Reconstructing Holocene temperatures in time and space using paleoclimate data assimilation. *Climate of the Past*, *18*(12), 2599–2629. https://doi.org/10.5194/cp-18-2599-2022

Fischer, H., Meissner, K. J., Mix, A. C., Abram, N. J., Austermann, J., Brovkin, V., et al. (2018). Palaeoclimate constraints on the impact of 2°C anthropogenic warming and beyond. *Nature Geoscience*, *11*(7), 474–485. https://doi.org/10.1038/s41561-018-0146-0

Fleitmann, D., Mudelsee, M., Burns, S. J., Bradley, R. S., Kramers, J., & Matter, A. (2008). Evidence for a widespread climatic anomaly at around 9.2 ka before present. *Paleoceanography*, *23*(1), 1–6. https://doi.org/10.1029/2007PA001519

Gajewski, K. (2015). Quantitative reconstruction of Holocene temperatures across the Canadian Arctic and Greenland. *Global and Planetary Change*, *128*, 14–23. https://doi.org/10.1016/j.gloplacha.2015.02.003

Grinsted, A., & Dahl-Jensen, D. (2002). A Monte Carlo-tuned model of the flow in the NorthGRIP area. *Annals of Glaciology*, *35*, 527–530. https://doi.org/10.3189/172756402781817130

Guillevic, M. (2013). Characterisation of rapid climate changes through isotope analyses of ice and entrapped air in the NEEM ice core. Climatology. University of Copenhagen, Faculty of Science, Denmark; Université de Versailles Saint Quentin En Yvelines (UVSQ), France, 2013. English., (September).

Hansen, K. E., Giraudeau, J., Wacker, L., Pearce, C., & Seidenkrantz, M. S. (2020). Reconstruction of Holocene oceanographic conditions in eastern Baffin Bay. *Climate of the Past*, *16*(3), 1075–1095. https://doi.org/10.5194/cp-16-1075-2020

Herron, B. M. M., & Langway, C. C. (1980). Firn densification: An empirical model. *Journal of Glaciology*, *25*(93), 373–385. https://doi.org/10.3189/s0022143000015239

Hwang, Y. T., & Frierson, D. M. W. (2010). Increasing atmospheric poleward energy transport with global warming. *Geophysical Research Letters*, *37*(24), 1–5. https://doi.org/10.1029/2010GL045440

Jaiser, R., Dethloff, K., Handorf, D., Rinke, A., & Cohen, J. (2012). Impact of sea ice cover changes on the northern hemisphere atmospheric winter circulation. *Tellus, Series A: Dynamic Meteorology and Oceanography*, *64*(1), 11595. https://doi.org/10.3402/tellusa.v64i0.11595

Kaufman, D. S., Ager, T. A., Anderson, N. J., Anderson, P. M., Andrews, J. T., Bartlein, P. J., et al. (2004). Holocene thermal maximum in the western Arctic (0-180°W). *Quaternary Science Reviews*, *23*(5–6), 529–560. https://doi.org/10.1016/j.quascirev.2003.09.007

Kaufman, D. S., & Broadman, E. (2023). Revisiting the Holocene global temperature conundrum. *Nature*, *614*(7948), 425–435. https://doi.org/10.1038/s41586-022-05536-w

Kaufman, D. S., McKay, N., Routson, C., Erb, M., Dätwyler, C., Sommer, P. S., et al. (2020). Holocene global mean surface temperature, a multi-method reconstruction approach. *Scientific Data*, *7*(1), 201. https://doi.org/10.1038/s41597-020-0530-7

Kindler, P., Guillevic, M., Baumgartner, M., Schwander, J., Landais, A., & Leuenberger, M. (2014). Temperature reconstruction from 10 to 120 kyr b2k from the NGRIP ice core. *Climate of the Past*, *10*(2), 887–902. https://doi.org/10.5194/cp-10-887-2014

Kobashi, T., Severinghaus, J. P., & Kawamura, K. (2008). Argon and nitrogen isotopes of trapped air in the GISP2 ice core during the Holocene epoch (0-11,500 B.P.): Methodology and implications for gas loss processes. *Geochimica et Cosmochimica Acta*, *72*(19), 4675–4686. https://doi.org/10.1016/j.gca.2008.07.006

Larocca, L. J., & Axford, Y. (2022). Arctic glaciers and ice caps through the Holocene:a circumpolar synthesis of lake-based reconstructions. *Climate of the Past*, *18*(3), 579–606. https://doi.org/10.5194/cp-18-579-2022

Lecavalier, B. S., Fisher, D. A., Milne, G. A., Vinther, B. M., Tarasov, L., Huybrechts, P., et al. (2017). High Arctic Holocene temperature record from the Agassiz ice cap and Greenland ice sheet evolution. *Proceedings of the National Academy of Sciences of the United States of America*, *114*(23), 5952–5957. https://doi.org/10.1073/pnas.1616287114

Lecavalier, B. S., Milne, G. A., Simpson, M. J. R., Wake, L., Huybrechts, P., Tarasov, L., et al. (2014). A model of Greenland ice sheet deglaciation constrained by observations of relative sea level and ice extent. *Quaternary Science Reviews*, *102*, 54–84. https://doi.org/10.1016/j.quascirev.2014.07.018

Lee, J. E., Edwards, J. S., Schmitt, J., Fischer, H., Bock, M., & Brook, E. J. (2020). Excess methane in Greenland ice cores associated with high dust concentrations. *Geochimica et Cosmochimica Acta*, *270*, 409–430. https://doi.org/10.1016/j.gca.2019.11.020

Legrain, E., Blard, P. H., Kageyama, M., Charreau, J., Leduc, G., Bourdin, S., & Bekaert, D. V. (2023). Moisture amplification of the high-altitude deglacial warming. *Quaternary Science Reviews*, *318*(May), 108303. https://doi.org/10.1016/j.quascirev.2023.108303

Liu, Y., Zhang, M., Liu, Z., Xia, Y., Huang, Y., Peng, Y., & Zhu, J. (2018). A possible role of dust in resolving the Holocene temperature conundrum. *Scientific Reports*, *8*(1), 1–9. https://doi.org/10.1038/s41598-018-22841-5

Liu, Z., Zhu, J., Rosenthal, Y., Zhang, X., Otto-Bliesner, B. L., Timmermann, A., et al. (2014). The Holocene temperature conundrum. *Proceedings of the National Academy of Sciences of the United States of America*, *111*(34). https://doi.org/10.1073/pnas.1407229111

Løkkegaard, A., Mankoff, K. D., Zdanowicz, C., Clow, G. D., Lüthi, M. P., Doyle, S. H., et al. (2023). Greenland and Canadian Arctic ice temperature profiles database. *The Cryosphere*, *17*(9), 3829–3845. https://doi.org/10.5194/tc-17-3829-2023

Loomis, S. E., Russell, J. M., Verschuren, D., Morrill, C., De Cort, G., Sinninghe Damsté, J. S., et al. (2017). The tropical lapse rate steepened during the Last Glacial Maximum. *Science Advances*, *3*(1), 1–7. https://doi.org/10.1126/sciadv.1600815

Lüning, S., & Vahrenholt, F. (2017). Paleoclimatological context and reference level of the 2°C and 1.5°C Paris agreement long-term temperature limits. *Frontiers in Earth Science*, *5*(December), 1–7. https://doi.org/10.3389/feart.2017.00104

Marcott, S. a., Shakun, J. D., Clark, P. U., & Mix, A. C. (2013). A reconstruction of regional and global temperatures for the past 11,300 years. *Science (New York, N.Y.)*, *339*(6124), 1198–1201. https://doi.org/10.1126/science.1228026

Marsicek, J., Shuman, B. N., Bartlein, P. J., Shafer, S. L., & Brewer, S. (2018). Reconciling divergent trends and millennial variations in Holocene temperatures. *Nature*, *554*(7690), 92–96. https://doi.org/10.1038/nature25464

Martin, K. C., Buizert, C., Brook, E. J., Williams, O. L., Edwards, J. S., Riddell-Young, B., et al. (2024). Mean annual temperature, methane, total air content, Delta 15N-N2, and Delta age from the Greenland ice sheet project two (GISP2), North Greenland Eemian ice drilling (NEEM), and North Greenland ice core project (NGRIP) ice cores, 0-18 thousand years before present. https://doi.org/10.18739/A2KP7TT2N

Martin, K. C., Buizert, C., Edwards, J. S., Kalk, M. L., Riddell-Young, B., Brook, E. J., et al. (2023). Bipolar impact and phasing of Heinrich-type climate variability. *Nature*, *617*(7959), 100–104. https://doi.org/10.1038/s41586-023-05875-2

Martinerie, P., Raynaud, D., Etheridge, D. M., Barnola, J. M., & Mazaudier, D. (1992). Physical and climatic parameters which influence the air content in polar ice. *Earth and Planetary Science Letters*, *112*(1–4), 1–13. https://doi.org/10.1016/0012-821x(92)90002-d

Masson-Delmotte, V., Kageyama, M., Braconnot, P., Charbit, S., Krinner, G., Ritz, C., et al. (2006). Past and future polar amplification of climate change: Climate model intercomparisons and ice-core constraints. *Climate Dynamics*, *26*(5), 513–529. https://doi.org/10.1007/s00382-005-0081-9

Masson-Delmotte, V., Steen-Larsen, H. C., Ortega, P., Swingedouw, D., Popp, T., Vinther, B. M., et al. (2015). Recent changes in north-west Greenland climate documented by NEEM shallow ice core data and simulations, and implications for past-temperature reconstructions. *The Cryosphere*, *9*(4), 1481–1504. https://doi.org/10.5194/tc-9-1481-2015

Miller, N. B., Turner, D. D., Bennartz, R., Shupe, M. D., Kulie, M. S., Cadeddu, M. P., & Walden, V. P. (2013). Surface-based inversions above central Greenland. *Journal of Geophysical Research: Atmospheres*, *118*(2), 495–506. https://doi.org/10.1029/2012JD018867

Mitchell, L., Brook, E., Lee, J. E., Buizert, C., & Sowers, T. (2013). Constraints on the late Holocene anthropogenic contribution to the atmospheric methane budget. *Science*, *342*(6161), 964–966. https://doi.org/10.1126/science.1238920

Osman, M. B., Tierney, J. E., Zhu, J., Tardif, R., Hakim, G. J., King, J., & Poulsen, C. J. (2021). Globally resolved surface temperatures since the last glacial maximum. *Nature*, *599*(7884), 239–244. https://doi.org/10.1038/s41586-021-03984-4

Oyabu, I., Kawamura, K., Kitamura, K., Dallmayr, R., Kitamura, A., Sawada, C., et al. (2020). New technique for high-precision, simultaneous measurements of CH4, N2O and CO2 concentrations; Isotopic and elemental ratios of N2, O2 and Ar; and total air content in ice cores by wet extraction. *Atmospheric Measurement Techniques*, *13*(12), 6703–6731. https://doi.org/10.5194/amt-13-6703-2020

Pepin, N., Bradley, R. S., Diaz, H. F., Baraer, M., Caceres, E. B., Forsythe, N., et al. (2015). Elevation-dependent warming in mountain regions of the world. *Nature Climate Change*, *5*(5), 424–430. https://doi.org/10.1038/nclimate2563

Rangwala, I., & Miller, J. R. (2012). Climate change in mountains: A review of elevation-dependent warming and its possible causes. *Climatic Change*, *114*(3–4), 527–547. https://doi.org/10.1007/s10584-012-0419-3

Rasmussen, S. O., Abbott, P. M., Blunier, T., Bourne, A. J., Brook, E., Buchardt, S. L., et al. (2013). A first chronology for the north Greenland Eemian ice drilling (NEEM) ice core. *Climate of the Past*, *9*(6), 2713–2730. https://doi.org/10.5194/cp-9-2713-2013

Raynaud, D., Lipenkov, V., Lemieux-Dudon, B., Duval, P., Loutre, M. F., & Lhomme, N. (2007). The local insolation signature of air content in Antarctic ice. A new step toward an absolute dating of ice records. *Earth and Planetary Science Letters*, *261*(3–4), 337–349. https://doi.org/10.1016/j.epsl.2007.06.025

Raynaud, D., Yin, Q., Capron, E., Wu, Z., Parrenin, F., Berger, A., & Lipenkov, V. (2023). Past Antarctic summer temperature revealed by total air content in ice cores, 1–17. https://doi.org/10.5194/egusphere-2023-2360

Rhodes, R. H., Faïn, X., Stowasser, C., Blunier, T., Chappellaz, J., McConnell, J. R., et al. (2013). Continuous methane measurements from a late Holocene Greenland ice core: Atmospheric and in-situ signals. *Earth and Planetary Science Letters*, *368*, 9–19. https://doi.org/10.1016/j.epsl.2013.02.034

Rosen, J. L., Brook, E. J., Severinghaus, J. P., Blunier, T., Mitchell, L. E., Lee, J. E., et al. (2014). An ice core record of near-synchronous global climate changes at the Bølling transition. *Nature Geoscience*, *7*(6), 459–463. https://doi.org/10.1038/ngeo2147

Seierstad, I. K., Abbott, P. M., Bigler, M., Blunier, T., Bourne, A. J., Brook, E., et al. (2014). Consistently dated records from the Greenland GRIP, GISP2 and NGRIP ice cores for the past 104 ka reveal regional millennial-scale δ18O gradients with possible Heinrich event imprint. *Quaternary Science Reviews*, *106*, 29–46. https://doi.org/10.1016/j.quascirev.2014.10.032

Sigl, M., Toohey, M., McConnell, J. R., Cole-Dai, J., & Severi, M. (2022). Volcanic stratospheric sulfur injections and aerosol optical depth during the Holocene (past 11 500 years) from a bipolar ice-core array. *Earth System Science Data*, *14*(7), 3167–3196. https://doi.org/10.5194/essd-14-3167-2022

Steffen, K., & Box, J. E. (2001). Surface climatology of the Greenland ice sheet: Greenland climate network 1995-1999. *Journal of Geophysical Research*, *106*(12), 33951–33964. https://doi.org/10.1029/2001jd900161

Svensson, A., Dahl-Jensen, D., Steffensen, J. P., Blunier, T., Rasmussen, S. O., Vinther, B. M., et al. (2020). Bipolar volcanic synchronization of abrupt climate change in Greenland and Antarctic ice cores during the last glacial period. *Climate of the Past*, *16*(4), 1565–1580. https://doi.org/10.5194/cp-16-1565-2020

Thompson, A. J., Zhu, J., Poulsen, C. J., Tierney, J. E., & Skinner, C. B. (2022). Northern Hemisphere vegetation change drives a Holocene thermal maximum. *Science Advances*, *8*(15), 2–11. https://doi.org/10.1126/sciadv.abj6535

Ullman, D. J., Carlson, A. E., Hostetler, S. W., Clark, P. U., Cuzzone, J., Milne, G. A., et al. (2016). Final Laurentide ice sheet deglaciation and Holocene climate-sea level change. *Quaternary Science Reviews*, *152*, 49–59. https://doi.org/10.1016/j.quascirev.2016.09.014

Veres, D., Bazin, L., Landais, A., Toyé Mahamadou Kele, H., Lemieux-Dudon, B., Parrenin, F., et al. (2013). The Antarctic ice core chronology (AICC2012): An optimized multi-parameter and multi-site dating approach for the last 120 thousand years. *Climate of the Past*, *9*(4), 1733–1748. https://doi.org/10.5194/cp-9-1733-2013

Vihma, T. (2014). Effects of Arctic sea ice decline on weather and climate: A review. *Surveys in Geophysics*, *35*(5), 1175–1214. https://doi.org/10.1007/s10712-014-9284-0

Vinther, B. M., Buchardt, S. L., Clausen, H. B., Dahl-Jensen, D., Johnsen, S. J., Fisher, D. A., et al. (2009). Holocene thinning of the Greenland ice sheet. *Nature*, *461*(7262), 385–388. https://doi.org/10.1038/nature08355

Vinther, B. M., Clausen, H. B., Fisher, D. A., Koerner, R. M., Johnsen, S. J., Andersen, K. K., et al. (2008). Synchronizing ice cores from the Renland and Agassiz ice caps to the Greenland ice core chronology. *Journal of Geophysical Research*, *113*(8), 1–10. https://doi.org/10.1029/2007JD009143

Willeit, M., Calov, R., Talento, S., Greve, R., Bernales, J., Klemann, V., et al. (2024). Glacial inception through rapid ice area increase driven by albedo and vegetation feedbacks. *Climate of the Past*, *20*(3), 597–623. https://doi.org/10.5194/cp-20-597-2024

Yang, X. Y., Fyfe, J. C., & Flato, G. M. (2010). The role of poleward energy transport in arctic temperature evolution. *Geophysical Research Letters*, *37*(14), 1–5. https://doi.org/10.1029/2010GL043934

Zhang, W., Wu, H., Cheng, J., Geng, J., Li, Q., Sun, Y., et al. (2022). Holocene seasonal temperature evolution and spatial variability over the Northern Hemisphere landmass. *Nature Communications*, *13*(1), 5334. https://doi.org/10.1038/s41467-022-33107-0

Zhang, Y., Renssen, H., Seppä, H., & Valdes, P. J. (2017). Holocene temperature evolution in the Northern Hemisphere high latitudes – Model-data comparisons. *Quaternary Science Reviews*, *173*, 101–113. https://doi.org/10.1016/j.quascirev.2017.07.018

Zhang, Y., Renssen, H., Seppä, H., & Valdes, P. J. (2018). Holocene temperature trends in the extratropical Northern Hemisphere based on inter-model comparisons. *Journal of Quaternary Science*, *33*(4), 464–476. https://doi.org/10.1002/jqs.3027

Zhang, Y., Seidel, D. J., Golaz, J. C., Deser, C., & Tomas, R. A. (2011). Climatological characteristics of Arctic and Antarctic surface-based inversions. *Journal of Climate*, *24*(19), 5167–5186. https://doi.org/10.1175/2011JCLI4004.1

Zheng, M., Sjolte, J., Adolphi, F., Møllesøe Vinther, B., Steen-Larsen, H. C., Popp, T. J., & Muscheler, R. (2018). Climate information preserved in seasonal water isotope at NEEM: Relationships with temperature, circulation and sea ice. *Climate of the Past*, *14*(7), 1067–1078. https://doi.org/10.5194/cp-14-1067-2018

## References From the Supporting Information

Petrenko, V. V., Severinghaus, J. P., Brook, E. J., Reeh, N., & Schaefer, H. (2006). Gas records from the West Greenland ice margin covering the Last Glacial Termination: A horizontal ice core. *Quaternary Science Reviews*, *25*(9–10), 865–875. https://doi.org/10.1016/j.quascirev.2005.09.005

Riddell-Young, B., Rosen, J., Brook, E., Buizert, C., Martin, K., Lee, J., et al. (2023). Atmospheric methane variability through the Last Glacial Maximum and deglaciation mainly controlled by tropical sources. *Nature Geoscience*, *16*(12), 1174–1180. https://doi.org/10.1038/s41561-023-01332-x

Severinghaus, J., Beaudette, R., Headly, M., Taylor, K., & Brook, E. (2009). Oxygen-18 of O2 Records the Impact of Abrupt Climate Change on the Terrestrial Biosphere. *Science*, *324*(June), 1431–1435. https://doi.org/10.4324/9781315841045

Sowers, T., Bender, M., & Raynaud, D. (1989). Elemental and isotopic composition of occluded O2 and N2 in polar ice. *Journal of Geophysical Research*, *94*(D4), 5137–5150. https://doi.org/10.1029/JD094iD04p05137